Microscopic dynamics in the liquid Li-Na alloy: An *ab initio* molecular dynamics study

D. J. González,[1,*] L. E. González,[2] J. M. López,[2] and M. J. Stott[1]
[1]*Department of Physics, Queen's University, Kingston, Ontario, Canada K7L 3N6*
[2]*Departamento de Física Teórica, Facultad de Ciencias, Universidad de Valladolid, 47011 Valladolid, Spain*
(Received 25 August 2003; revised manuscript received 20 November 2003; published 31 March 2004)

We present results for several structural and dynamical properties of the liquid $Li_{1-x}Na_x$ alloy. The study has been carried out by means of the orbital-free *ab initio* molecular dynamics method, combined with local ionic pseudopotentials constructed within the same framework. We obtain good agreement with the available experimental data, reproducing accurately, the strong homocoordinating tendencies exhibited by this alloy. The calculated partial dynamic structure factors exhibit clear side peaks whose frequencies, for $q \leqslant 0.25$ Å^{-1}, correspond to the hydrodynamic sound dispersion of the binary alloy, whereas for larger q values fast and slow sound modes are identified. The mass ratio in this system, $m_{\mathrm{Na}}/m_{\mathrm{Li}} \approx 3$, is the smallest one so far for which the fast mode is observed.

DOI: 10.1103/PhysRevE.69.031205 PACS number(s): 61.20.Ja, 61.25.Mv, 71.15.Pd

I. INTRODUCTION

Molecular dynamics (MD) has become a useful technique to study the properties of liquid systems. Whereas classical molecular dynamics (CMD) techniques require interatomic potentials, the *ab initio* molecular dynamics (AIMD) methods compute the forces acting on the nuclei from electronic structure calculations performed as the MD trajectory is generated; therefore the nuclear positions evolve according to classical mechanics while the electronic subsystem follows adiabatically.

Density functional theory (DFT) [1,2] underlies many AIMD methods. However, when the Kohn-Sham (KS) orbital representation of DFT is used (KS-AIMD methods), the computational demands become very heavy, limiting the sizes of the systems to be studied and the simulation times; for example, previous studies of liquid metals and alloys [3–6] have used around 100 atoms and simulation times between 2–5 ps. These limitations can be partly overcome by the so-called orbital-free *ab initio* molecular dynamics (OF-AIMD) method, which uses an approximate form for the electronic kinetic energy, but no longer requires the orbitals of the KS formulation. Consequently, the number of variables and the computational time for a simulation are greatly reduced, enabling the study of larger samples (several hundreds of particles) and for longer simulation times (tens of ps).

Research into the dynamical properties of liquid metals has already produced much experimental and theoretical work [7]. Inelastic neutron scattering (INS) has been the usual experimental technique for studying the dynamics of condensed matter at the kinetic region. Moreover, it has been recently supplemented by high resolution inelastic x-ray scattering (IXS) which overcomes the kinematic limitations of INS techniques. With a proper separation procedure INS provides in principle information on both the coherent and incoherent contributions to the inelastic scattering cross section, whereas IXS can only access the coherent part. In addition, theoretical developments such as the memory function formalism or the kinetic theory, along with the realization that the decay of several time-dependent properties can be linked to the interplay of two different dynamical processes, has created a theoretical framework whose application to simple liquids has led to good qualitative results for several dynamical magnitudes [7–9].

Less effort has been devoted to liquid binary alloys, but, starting with the pioneering MD studies on liquid Na-K [10], and liquid Li_4Pb [11], where a high-frequency mode supported by the Li atoms only (''fast sound'') was found, several theoretical [12–14], computer simulations [15–21], and experimental [21–24] studies have investigated the collective excitations in liquid binary systems.

On the theoretical side the application of kinetic theory, namely, the revised Enskog theory (RET) to a model binary mixture of hard spheres [12,13], and the recent generalized collective model (GCM) approach [14] have given useful insights into the nature of the collective excitations, particularly the longitudinal ones. The transverse dynamics has received less attention because it is not visible in scattering experiments and only the MD simulations can provide information on it. The recent application of the GCM approach, which combines MD simulations with the memory function formalism, to binary Lennard-Jones fluids and liquid alloys has revealed the existence of transverse optic modes, which arise in connection with the concentration fluctuations.

In this paper we present an AIMD study on the structural and dynamical properties of the liquid $Li_{1-x}Na_x$ alloy. This is a typical phase separating system with a phase diagram dominated by a region of two immiscible liquids. The phase separation curve has been experimentally determined [25–27] and shows a consolute point at $T \approx 577$ K and composition $x_{\mathrm{Li}} \approx 0.64$; this is close to the ''zero alloy'' composition ($x_{\mathrm{Li}} \approx 0.61$) for which the total static structure factor $S_T(q)$ reduces to the concentration-concentration partial structure factor, namely, $S_T(q) = S_{\mathrm{CC}}(q)/x_{\mathrm{Li}}x_{\mathrm{Na}}$, because of the negative scattering length of the ^{7}Li isotope. $S_T(q)$ has been measured [28] for several compositions, and temperatures in the range 590 K–725 K, whereas INS experiments [29] have

*On leave from: Departamento de Física Teórica, Facultad de Ciencias, Universidad de Valladolid, 47011 Valladolid, Spain.

been performed for the zero alloy only. The experimental $S_T(q)$ for the zero alloy is dominated by strong small-angle scattering, which is a typical characteristic of a phase separating system, and the oscillations of $S_T(q)$ beyond the small-angle region are rather weak, with a characteristic ripple around $q \approx 2.2$ Å^{-1}. The simultaneous reproduction of these structural features has become an objective of most theoretical studies, which have used either semiempirical [30,31] or more fundamental [6,32–37] approaches. Recently, Canales *et al.* [36] have obtained a very satisfactory description of the static structure of the zero alloy by using CMD combined with interatomic pair potentials derived within the neutral pseudoatom method (NPA) [38]. These same potentials have also been used in a study of the dynamic properties of the zero alloy [39] by CMD, leading to results in good agreement with the experimental measurements.

Recently, two KS-AIMD simulations have investigated the static structure of this alloy. Hoshino and co-workers [5] used 100 atoms, an energy cutoff of 10 Ry, and their $S_T(q)$ reproduces the main experimental trends, although the results are extremely noisy. Also, Costa Cabral *et al.* [6] used 108 atoms, an energy cutoff of 9 Ry, and obtained properties averaged over 400 configurations. The resulting $S_T(q)$ is in good agreement with experiment, although the short simulation time obviously precludes the study of the dynamical magnitudes, except for the diffusion coefficients (DC's).

We have recently reported two other OF-AIMD calculations for the zero alloy at 590 K [19,20], leading to excellent agreement with the experimental static structure, and showing the appearance of a fast sound mode and its merging with the hydrodynamic mode for small wave vectors. In this paper we extend the simulations to other concentrations and temperatures and study a variety of dynamic properties, including both single particle and collective magnitudes, which are amenable to study because of the possibility of running long simulations with a large number of configurations.

II. THEORY

A liquid simple metal alloy, A_xB_{1-x}, can be regarded as an assembly of N_A, *A*-type, and N_B, *B*-type, bare ions with charges Z_v^A and Z_v^B, respectively, interacting with $N_e = N_A Z_v^A + N_B Z_v^B$ valence electrons through electron-ion potentials $v_A(r)$ and $v_B(r)$. The total potential energy of the system can be written as the sum of the direct ion-ion interaction energy plus the ground state energy of the electronic system subject to the external potential created by the ions, $V_{\rm ext}(\vec{r},\{\vec{R}_l\}) = \Sigma_{i=A,B}\Sigma_{l(i)} v_i(|\vec{r}-\vec{R}_l|)$,

$$E(\{\vec{R}_l\}) = \frac{1}{2}\sum_{i,j=A,B}\sum_{l(i)\neq m(j)}\frac{Z_i Z_j}{|\vec{R}_l-\vec{R}_m|} + E_g[\rho_g(\vec{r}), V_{\rm ext}(\vec{r},\{\vec{R}_l\})], \quad (1)$$

where $\vec{R}_l$ are the ionic positions, the sum over $l(i)$ extends over the sites occupied by the *i*-type ions, and $\rho_g(\vec{r})$ is the ground state electronic density. According to DFT, $\rho_g(\vec{r})$ can be obtained by minimizing the energy functional

$$E[\rho(\vec{r})] = T_s[\rho] + E_{\rm ext}[\rho] + E_H[\rho] + E_{\rm xc}[\rho], \quad (2)$$

where the terms represent, respectively, the electronic kinetic energy $T_s[\rho]$ of a noninteracting system with density $\rho(\vec{r})$, the energy of interaction with the external potential due to the ions, $E_{\rm ext}[\rho]$, the classical electrostatic energy (Hartree term) $E_H[\rho]$, and the exchange-correlation energy $E_{\rm xc}[\rho]$, for which we will adopt the local density approximation.

Within the KS-AIMD approach the electronic density is described in terms of orbitals and $T_s[\rho]$ is calculated exactly, although with a large computational effort. This obstacle can be reduced somewhat by adopting the OF-AIMD approach where an explicit but approximate density functional for $T_s[\rho]$ is used [40]. In this work we have used for $T_s[\rho]$ a simplified version of an expression proposed by García-González *et al.* [41], namely, $T_s = T_W + T_\beta$, where T_W is the von Weizsacker term, and

$$T_\beta = \frac{3}{10}\int d\vec{r}\,\rho(\vec{r})^{5/3-2\beta}\tilde{k}(\vec{r})^2, \quad (3)$$

$$\tilde{k}(\vec{r}) = (2k_F^0)^3 \int d\vec{s}\,k(\vec{s}) w_\beta(2k_F^0|\vec{r}-\vec{s}|), \quad (4)$$

where $k(\vec{r}) = (3\pi^2)^{1/3}\rho(\vec{r})^\beta$, k_F^0 is the Fermi wave vector corresponding to a mean electron density ρ_0, and $w_\beta(x)$ is a weight function determined by requiring the correct recovery of both the linear response and the uniform density limits [40]. This functional is positive definite for any value of β, which is an essential requirement in a variational calculation. In these simulations we have used a value of $\beta = 0.51$ for reasons discussed elsewhere [43].

The construction of the ion pseudopotentials, $v_{\rm ps}^\alpha(\vec{r})$, used for the ion-electron interaction is described fully in Refs. [19,44]. The pseudopotentials are local and are constructed from first principles by fitting to a model of an ion immersed in a metallic medium.

Technical details

We have considered 2000 ions in a cubic cell with periodic boundary conditions. Given the ionic positions at time *t*, the electronic energy functional is minimized with respect to $\rho(\vec{r})$ represented by a single *effective orbital* $\psi(\vec{r})$ defined as $\rho(\vec{r}) = \psi(\vec{r})^2$. The orbital is expanded in plane waves truncated at a cutoff energy $E_{\rm Cut} = 8$ Ry for all the concentrations considered. The energy minimization with respect to the Fourier coefficients of the expansion is performed every time step using a quenching method which results in the ground state electronic density and energy. The forces on the ions are obtained from the electronic ground state via the Hellman-Feynman theorem, and the ionic positions and velocities are updated by solving Newton's equations, with the Verlet leap-frog algorithm with a time step of 2.5×10^{-3} ps. In the simulations equilibration took 5 ps and the calculation of properties was made averaging over 50 ps.

The calculation of the time correlation functions (CF) was performed by taking time origins every five time steps. Several CF depend on the wave vector $\vec{q}$, though in fact, as the

TABLE I. Input data for the series Li-Na at $T=590$ K, studied in this work, along with some simulation details. The numbers in parenthesis correspond to $T=725$ K. ρ is the total ionic number density taken from Ref. [42] and N the number of particles.

$x=x_{\mathrm{Na}}$	ρ (Å^{-3})	N
0.0	0.04330	600
0.20	0.036819	2000
0.39	0.032180	2000
	(0.031085)	(600)
0.60	0.028241	2000
1.0	0.022960	600

real system is isotropic, they depend only on $q\equiv|\vec{q}|$. For a given q value, N_q vectors exist with the same modulus and the final result of the CF is an average over these N_q directions. In our calculations, $N_q=3$ for the smallest q (≈ 0.16 Å^{-1}) whereas for the greater wave vectors selected for our calculations, N_q takes a maximum value of 24.

III. RESULTS

The liquid $\mathrm{Li}_{1-x}\mathrm{Na}_x$ alloy has been simulated at $T=590$ K and concentrations $x_{\mathrm{Na}}=0.2$, 0.39, and 0.60, and $T=725$ K for $x_{\mathrm{Na}}=0.39$, with total ionic number densities taken from the experimental data of Jost *et al.* [42]. Table I shows the thermodynamic states considered in this study.

A. Structural properties

The simulations allow a direct evaluation of the partial pair distribution functions $g_{ij}(r)$, as well as the corresponding partial Ashcroft-Langreth (AL) structure factors, $S_{ij}(q)$. Figure 1 shows the calculated $g_{ij}(r)$. The changes with concentration of $g_{\mathrm{LiLi}}(r)$ are more marked than those of $g_{\mathrm{LiNa}}(r)$ and $g_{\mathrm{NaNa}}(r)$. With increasing Na concentration the height of the main peak of $g_{\mathrm{LiLi}}(r)$ increases, whereas that of $g_{\mathrm{LiNa}}(r)$ is practically unchanged and that of $g_{\mathrm{NaNa}}(r)$ decreases. For all concentrations, $g_{\mathrm{LiNa}}(r)$ remains smaller than the average of $g_{\mathrm{LiLi}}(r)$ and $g_{\mathrm{NaNa}}(r)$ suggesting the homocoordinating tendencies in the alloys. A simple, quantitative analysis of the short range order in the alloy is provided by the Warren-Cowley [45–47] short range order (SRO) parameter for the first neighbor shell, $\alpha_1^{(i)}$, defined as

$$\alpha_1^{(i)}=1-\frac{n_{ij}}{x_j(n_{ii}+n_{ij})} \quad (j\neq i=1,2), \tag{5}$$

where x_j is the concentration of the j-type particles and n_{ij} is the number of j-type particles around an i-type particle, within a sphere of radius R_{ij}. n_{ij} can be calculated from the partial pair distribution functions, $g_{ij}(r)$, as follows:

$$n_{ij}=4\pi\rho x_j\int_0^{R_{ij}} r^2 g_{ij}(r)\,dr, \tag{6}$$

where R_{ij} is usually taken to be [48] the position of the first minimum of the corresponding $g_{ij}(r)$. For a random distribution of atoms $\alpha_1^{(i)}=0$, whereas a positive (negative) value for $\alpha_1^{(i)}$ suggests a homocoordinating (heterocoordinating) tendency. We have evaluated both $\alpha_1^{(\mathrm{Li})}$ and $\alpha_1^{(\mathrm{Na})}$ for the liquid $\mathrm{Li}_x\mathrm{Na}_{1-x}$ alloy at $T=590$ K. The results shown in Table II clearly confirm the segregating tendency. Moreover, the results for $T=725$ K show that as temperature increases, the segregating tendency weakens.

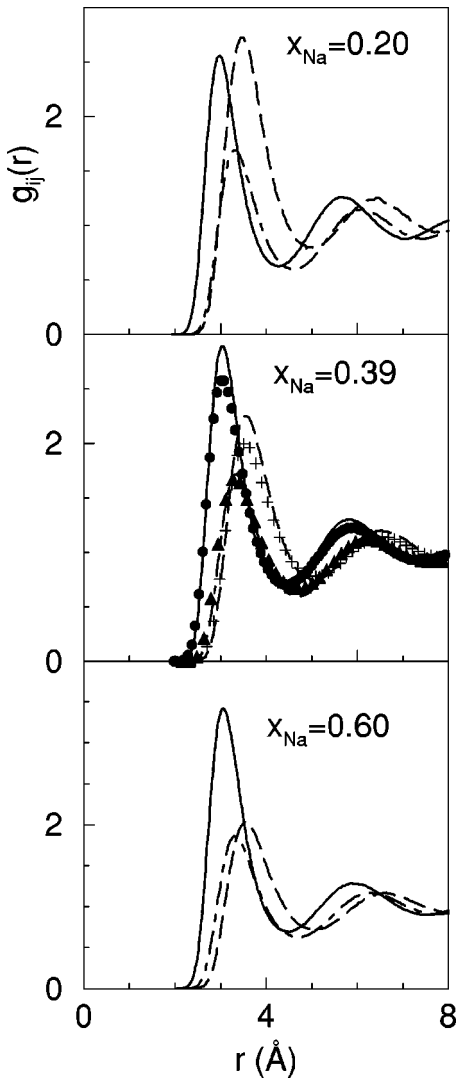

FIG. 1. Partial pair distribution functions, $g_{ij}(r)$, for the liquid Li-Na alloy at $T=590$ K and three concentrations. The full, dashed, and dot-dashed lines represent $g_{\mathrm{LiLi}}(r)$, $g_{\mathrm{NaNa}}(r)$, and $g_{\mathrm{LiNa}}(r)$, respectively. For $x_{\mathrm{Na}}=0.39$ the symbols denote the pair distribution functions at $T=725$ K.

Ruppersberg and Knoll [28] have measured, by neutron diffraction, the total static structure factor at $T=590$ K and $x_{\mathrm{Na}}=0.20$, 0.39, and 0.60 as well as for $T=725$ K and $x_{\mathrm{Na}}=0.39$. The experimental static structure factors, $S_T^{\mathrm{expt}}(q)$, have some common features, namely, (i) a rapid increase of $S_T^{\mathrm{expt}}(q)$ as $q\to 0$, (ii) extremely weak oscillations beyond $q\geqslant 2.0$ Å^{-1}, which is characteristic of alloys with weak chemical ordering, (iii) at the zero alloy composition, $\mathrm{Li}_{0.61}\mathrm{Na}_{0.39}$, there appears a characteristic ripple with two peaks at $q\approx 2.0$ and ≈ 2.25 Å^{-1}, respectively.

TABLE II. Calculated values of coordination numbers, n_{ij}, and the Warren-Cowley SRO parameters, $\alpha_1^{(i)}$, for the Li-Na liquid alloy at $T=590$ K. The numbers in parentheses correspond to $T=725$ K.

x_{Na}	n_{LiLi}	n_{LiNa}	n_{NaLi}	n_{NaNa}	$\alpha_1^{(Li)}$	$\alpha_1^{(Na)}$
0.20	10.3	2.4	9.8	4.7	0.06	0.16
0.39	8.3(8.0)	4.3(4.5)	6.7(7.0)	7.3(6.9)	0.12(0.08)	0.21(0.17)
0.60	5.76	6.5	4.3	9.1	0.12	0.20

Figure 2 shows a comparison, for three concentrations at $T=590$ K, between $S_T^{expt}(q)$ and the corresponding OF-AIMD simulation results. The agreement between experiment and simulation is very satisfactory, with the OF-AIMD simulations reproducing rather well all the basic features of $S_T^{expt}(q)$: an increase as $q\to 0$, and the position and amplitude of the oscillations. Moreover, the two peaks at $q\approx 2$ and 2.5 $Å^{-1}$ for the $Li_{0.61}Na_{0.39}$ alloy are also well reproduced.

The KS-AIMD simulations of Costa Cabral and Martins [6] for the $Li_{0.61}Na_{0.39}$ alloy follow the trend of $S_T^{expt}(q)$, although the ripple is somewhat underestimated, possibly due to the small number of configurations and/or particles used in the simulation. Their results are shown in Fig. 2 along with those from the KS-AIMD simulations of Hoshino *et al.* [5] which have a much greater statistical noise.

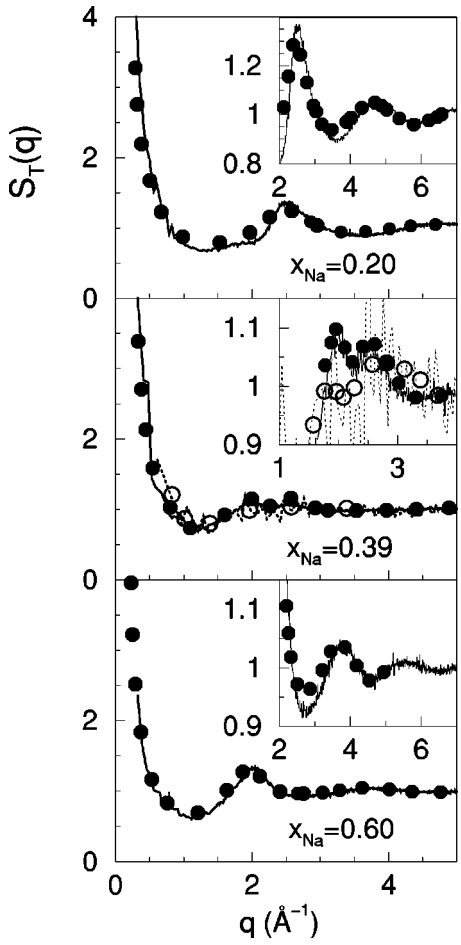

FIG. 2. Total static structure factor $S_T(q)$ for the liquid Li-Na alloy at $T=590$ K and three concentrations. Continuous lines are the results from the present OF-AIMD simulations whereas the full circles are the experimental neutron diffraction data of Ruppersberg and Knoll [28]. In the figure for $x_{Na}=0.39$, the dotted line and the open circles are the KS-AIMD results of Hoshino *et al.* [5], and Costa Cabral and Martins [6], respectively. The insets show the main peaks region expanded.

The analysis of the ordering tendencies in a liquid alloy is more conveniently performed in terms of the Bhatia-Thornton (BT) partial structure factors [49]. For a binary alloy these are (C denotes concentration N denotes number)

$$S_{CC}(q)=x_1x_2[x_2S_{11}(q)+x_1S_{22}(q)-2(x_1x_2)^{1/2}S_{12}(q)],$$

$$S_{NN}(q)=x_1S_{11}(q)+x_2S_{22}(q)+2(x_1x_2)^{1/2}S_{12}(q),$$

$$S_{NC}(q)=S_{11}(q)-S_{22}(q)+(x_2-x_1)/(x_1x_2)^{1/2}S_{12}(q),$$

where $S_{ij}(q)$ are the partial AL structure factors. The long-wavelength limits of the BT partial structure factors are related to thermodynamic quantities and also provides information on the short range order. In the present system, the experimental $S_{CC}^{expt}(q\to 0)$ take substantial values for all concentrations, indicating strong homocoordinating tendencies, and this tendency is satisfactorily described by the present OF-AIMD simulations for small q.

B. Dynamic properties

1. Single-particle dynamics

For liquid systems, information about several transport properties related to the mobility of particles and the coupling between the velocities of distinct particles is provided by some time correlation functions among the atomic velocities. These functions cannot be determined experimentally and other methods, such as MD simulations, must be used. Here, we present results for the relative velocity correlation functions (VCF), $Z_{ij}(t)$, which are defined [50] as the time correlation function of the relative velocity of the center of mass of species i with respect to the center of mass of species j,

$$Z_{ij}(t)=\tfrac{1}{3}x_ix_jN\langle[\vec{u}_i(t)-\vec{u}_j(t)]\cdot[\vec{u}_i(0)-\vec{u}_j(0)]\rangle, \quad (7)$$

where N is the total number of particles and $\vec{u}_i(t)$ is the mean velocity of component i,

$$\vec{u}_i(t)\equiv N_i^{-1}\sum_{l(i)=1}^{N_i}\vec{u}_{l(i)}(t), \quad (8)$$

with N_i being the total number of i-type particles and $\vec{u}_{l(i)}(t)$ the velocity of the i-type particle $l(i)$. $Z_{ij}(t)$ can be separated into self, $Z^0_{ij}(t)$, and distinct, $Z^d_{ij}(t)$, contributions as follows:

$$Z_{ij}(t)=(1-\delta_{ij})Z^0_{ij}(t)+x_i x_j Z^d_{ij}(t), \tag{9}$$

where δ_{ij} is Kronecker's delta, with $Z^0_{ij}(t)=x_j Z^s_i(t)+x_i Z^s_j(t)$, $Z^s_i(t)$ stands for the well-known velocity autocorrelation function of a tagged i-type particle in the fluid, whereas $Z^d_{ij}(t)$ account for the contribution of the distinct velocity correlations. The time integrals of $Z_{ij}(t)$, $Z^0_{ij}(t)$, $Z^d_{ij}(t)$, and $Z^s_i(t)$ give the associated DC's, namely, D_{ij}, D^0_{ij}, D^d_{ij}, and D^s_i respectively, where D^s_i is the standard self-diffusion coefficient. For binary mixtures we may write

$$D_{12}=D^0_{12}+x_1x_2D^d_{12}\equiv D^0_{12}(1+\gamma_{12}), \tag{10}$$

with $D^0_{12}=x_2D^s_1+x_1D^s_2$ and γ_{12} is a measure of the deviation from an ideal mixture (when all species are identical, $\gamma_{12}=0$). Also, within this formalism, the interdiffusion coefficient is written as

$$D_{\rm int}=\theta D_{12}\equiv\theta(1+\gamma_{12})D^0_{12}, \tag{11}$$

where $\theta=x_1x_2/S_{\rm CC}(q\to0)$. For a nearly ideal mixture, $\theta\approx1$, $\gamma_{12}\approx0$, and therefore $D_{\rm int}\approx D^0_{12}$.

The results obtained for the self, relative, and distinct VCF's in the $Li_{1-x}Na_x$ liquid alloy are shown in Fig. 3, where for comparison we have also plotted the VCF's for both pure Li and Na at $T=590$ K and number densities at their corresponding coexisting lines (see Table I). $Z^s_{\rm Li}(t)$ and $Z^s_{\rm Na}(t)$ have shapes (i.e., rate of decay and depth of first minimum) similar to the pure components although with some differences due to the variations in the total ionic number density as the concentration is varied. Notice that when going from pure Na to pure Li, the total number density changes by $\approx$100%. As $x_{\rm Na}$ is decreased, the total ionic number density is increased, which implies that the Na ions experience an increased rate of collisions (as compared with the pure Na case) and therefore their correlation time is decreased. This effect is reflected in a somewhat faster decrease (as compared with pure Na) of $Z^s_{\rm Na}(t)$ and a smaller $D^s_{\rm Na}$ when $x_{\rm Na}$ is decreased. On the other hand, just the opposite behavior is exhibited by both $Z^s_{\rm Li}(t)$ and $D^s_{\rm Li}$.

$Z^d_{\rm LiNa}(t)$ accounts for the effects of distinct correlations, either with particles of the same or different species. A quantitative measure of the distinct effects is given by $\gamma_{\rm LiNa}$, defined in Eq. (10), which as shown in Table III, takes substantial positive values. This indicates [50,51] that particles of the same species have a greater tendency to diffuse together than those of distinct species. This is another indicator of homocoordinating tendencies in the alloy which are stronger, in accordance with experiment, at $x_{\rm Na}\approx0.39$, where the values of both $\gamma_{\rm LiNa}$ and $D^d_{\rm LiNa}$ reach a maxima.

Unfortunately, the experimental determination of the self-diffusion coefficients in metallic melts is rather difficult and, to the best of our knowledge, results are only available for the $Na_{0.32}K_{0.68}$ system [52]. However, to give some indication of the accuracy of our results for the alloys, we have evaluated the self-diffusion coefficients of the pure components at 590 K. The calculation has been performed using their respective VCF's with the results $D^0_{\rm Na}=1.22$ and $D^0_{\rm Li}=1.13$ (in 10^{-4} cm^2/s units). The corresponding experimental values are $D^{\rm expt}_{\rm Na}=1.24\pm0.20$ [53] but for Li several values are available which lie within the range 1.02–1.27 ± 0.20 [53,54].

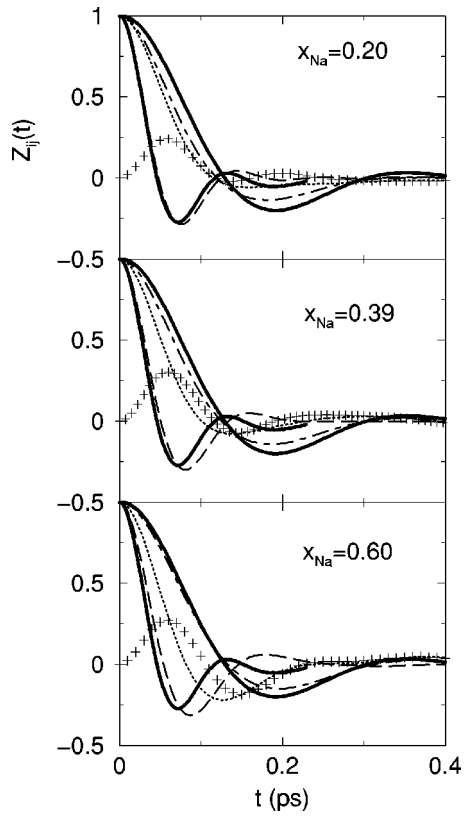

FIG. 3. Normalized relative, self, and distinct VCF's for the liquid Li-Na alloy at $T=590$ K and three concentrations. The dotted, pluses, dashed, and dot-dashed lines represent $Z_{\rm LiNa}(t)$, $x_{\rm Li}x_{\rm Na}Z^d_{\rm LiNa}(t)$, $Z^s_{\rm Li}(t)$, and $Z^s_{\rm Na}(t)$, respectively. The full thick lines represent the VACF's of pure Li (fast decay) and Na (slower decay) at $T=590$ K.

Table III includes the results for $S_{\rm CC}(q\to0)D_{\rm int}$. The results using Darken's semiempirical expression [55], $S_{\rm CC}(q$

TABLE III. Diffusion coefficients (in 10^{-4} cm^2/s) and related magnitudes, for the Li-Na liquid alloy at $T=590$ K. The numbers in parenthesis correspond to $x_{\rm Na}=0.39$ at $T=725$ K.

$x_{\rm Na}$	0.20	0.39	0.60
$D^s_{\rm Li}$	1.17	1.22 (1.87)	1.25
$D^s_{\rm Na}$	1.04	1.15 (1.75)	1.23
$D_{\rm LiNa}$	1.48	2.00 (2.45)	1.80
$D^0_{\rm LiNa}$	1.06	1.18 (1.79)	1.26
$D^d_{\rm LiNa}$	2.62	3.50 (2.76)	2.25
$\gamma_{\rm LiNa}$	0.40	0.71 (0.37)	0.43
$S_{\rm CC}(0)D_{\rm int}$	0.26	0.48 (0.58)	0.46
$S_{\rm CC}(0)D^{\rm (Darken)}_{\rm int}$	0.17	0.28 (0.43)	0.30

$\rightarrow 0) D_{\rm int} = x_1 x_2 D_{12}^0$, are nearly 50% smaller than those from the OF-AIMD. This is another manifestation of the important role played in this alloy by the distinct interparticle velocity correlations which are neglected in Darken's relation.

2. Collective dynamics

The collective dynamics of density fluctuations in an alloy is usually described through the partial AL intermediate scattering functions, $F_{ij}(\vec{q},t) = \langle \rho_i(\vec{q},t) \rho_j^*(\vec{q},0) \rangle$, where

$$\rho_j(\vec{q},t) = \frac{1}{\sqrt{N_j}} \sum_{l(j)=1}^{N_j} \exp[i\vec{q} \cdot \vec{R}_{l(j)}(t)] \tag{12}$$

is the Fourier transform (FT) of the j-type component partial number density, N_j is the number of j-type particles, $\vec{R}_{l(j)}(t)$ is the position of the j-type particle l, and $\langle \cdots \rangle$ denotes the ensemble average. The time FT of $F_{ij}(\vec{q},t)$ into the frequency domain gives the partial dynamic structure factors $S_{ij}(\vec{q},\omega)$ which are directly connected with the inelastic neutron scattering data.

Another important dynamical quantity is the j-type component particle current defined as

$$\vec{j}_j(\vec{q},t) = \frac{1}{\sqrt{N_j}} \sum_{l(j)=1}^{N_j} \vec{u}_{l(j)}(t) \exp[i\vec{q} \cdot \vec{R}_{l(j)}(t)], \tag{13}$$

which is usually split into a longitudinal component $j_j^L(\vec{q},t)$, parallel to $\vec{q}$, and a transverse component $j_j^T(\vec{q},t)$, perpendicular to $\vec{q}$. The partial longitudinal, $C_{ij}^L(\vec{q},t)$, and transverse, $C_{ij}^T(\vec{q},t)$, current correlation functions are defined in terms of these:

$$C_{ij}^L(\vec{q},t) = \langle j_i^L(\vec{q},t) j_j^{L*}(\vec{q},0) \rangle, \tag{14}$$

$$C_{ij}^T(\vec{q},t) = \tfrac{1}{2} \langle j_i^T(\vec{q},t) j_j^{T*}(\vec{q},0) \rangle,$$

and their time FT's give the respective spectra, $C_{ij}^L(\vec{q},\omega)$ and $C_{ij}^T(\vec{q},\omega)$. Finally, for isotropic systems, all the previous correlation functions depend on $q = |\vec{q}|$ only.

The partial AL scattering functions, $F_{\rm LiLi}(q,t)$, $F_{\rm NaNa}(q,t)$, and $F_{\rm LiNa}(q,t)$, as well as the BT ones $F_{\rm NN}(q,t)$, $F_{\rm NC}(q,t)$, and $F_{\rm CC}(q,t)$ are shown in Figs. 4 and 5 at two q values. $F_{\rm LiLi}(q,t)$, $F_{\rm NaNa}(q,t)$, $F_{\rm NN}(q,t)$ and $F_{\rm CC}(q,t)$ are always positive, whereas the $F_{\rm LiNa}(q,t)$ and $F_{\rm NC}(q,t)$ can be either positive or negative, because $F_{ij}(q,t=0) = S_{ij}(q)$ and both $S_{\rm LiNa}(q)$ and $S_{\rm NC}(q)$ oscillate around zero. $F_{ij}(q,t)$ go monotonically to zero, showing slower decays as q decreases; moreover this long-time behavior is reflected in their corresponding $S_{ij}(q,\omega=0)$, as observed in Figs. 6 and 7.

The partial dynamic structure factors, $S_{ij}(q,\omega)$, give information about the possible existence of propagating longitudinal modes. Figures 6 and 7 show, for two q values, the calculated $S_{\rm LiLi}(q,\omega)$, $S_{\rm NaNa}(q,\omega)$, $S_{\rm NN}(q,\omega)$, and $S_{\rm CC}(q,\omega)$. For the three concentrations, at low q values, $S_{\rm LiLi}(q,\omega)$, $S_{\rm NaNa}(q,\omega)$, and $S_{\rm NN}(q,\omega)$ exhibit clear side peaks at very similar frequencies, which is the typical behavior in the hydrodynamic regime and represents a propagating acoustic mode. This is clearly reflected in $S_{\rm NN}(q,\omega)$ which accounts for the average behavior of the system and in the hydrodynamic regime exhibits a clear Rayleigh-Brillouin structure [56], similar to the dynamic structure factor in one-component liquids. From the position of the observed Brillouin peaks at the smallest q value allowed by the simulations ($q_{\rm min} \approx 0.151$, 0.158, and 0.165 Å^{-1} for $x_{\rm Na} = 0.60$, 0.39, and 0.20, respectively) we can estimate the adiabatic velocity of propagation, $c_s = \omega_B / q$, where ω_B stands for the position of the Brillouin peak. For $x_{\rm Na} = 0.20$, $S_{\rm NN}(q,\omega)$ at $q_{\rm min}$ shows a clear Brillouin peak at $\omega_B \approx 5.1$ ps^{-1}, which leads to a $c_s = 3100$ m/s; similarly, we obtain $c_s = 2530$ m/s for $x_{\rm Na} = 0.60$ and $c_s = 3000$ m/s for $x_{\rm Na} = 0.39$. Moreover, for this latter concentration at $T = 725$ K we obtain a lower value of $c_s = 2750$ m/s. We are not aware of any experimental measurement of the adiabatic sound velocity in this alloy; however, data are available (at $T = 590$ K) for the limits $x_{\rm Na} = 1$ (pure Na) and $x_{\rm Na} = 0$ (pure Li), where the OF-AIMD calculations give $c_s = 2330 \pm 80$ m/s and c_s

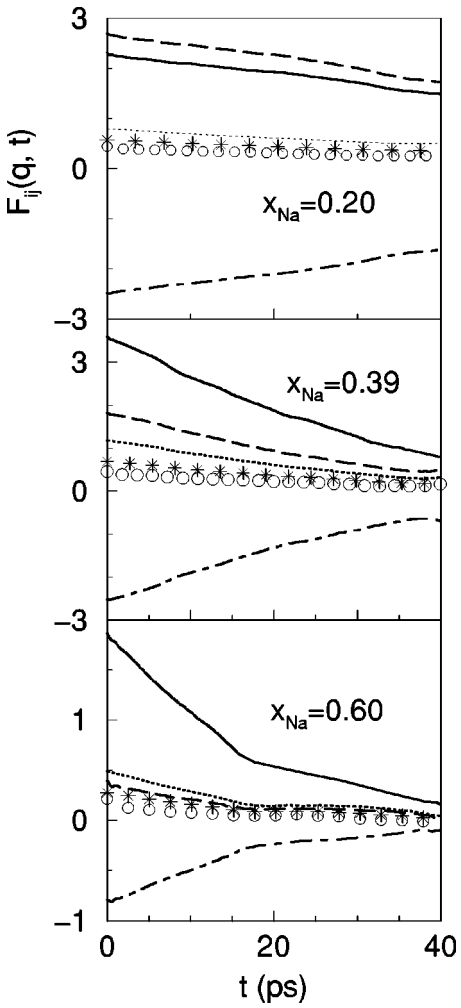

FIG. 4. Partial intermediate scattering functions, $F_{ij}(q,t)$, at $q = 0.23$ Å^{-1}, for the liquid Li-Na alloy at $T = 590$ K and three concentrations. Full line—$F_{\rm LiLi}(q,t)$, dashed line—$F_{\rm NaNa}(q,t)$, dot-dashed line—$F_{\rm LiNa}(q,t)$, open circles—$F_{\rm NN}(q,t)$, stars—$F_{\rm NC}(q,t)$, and dotted line—$F_{\rm CC}(q,t)$.

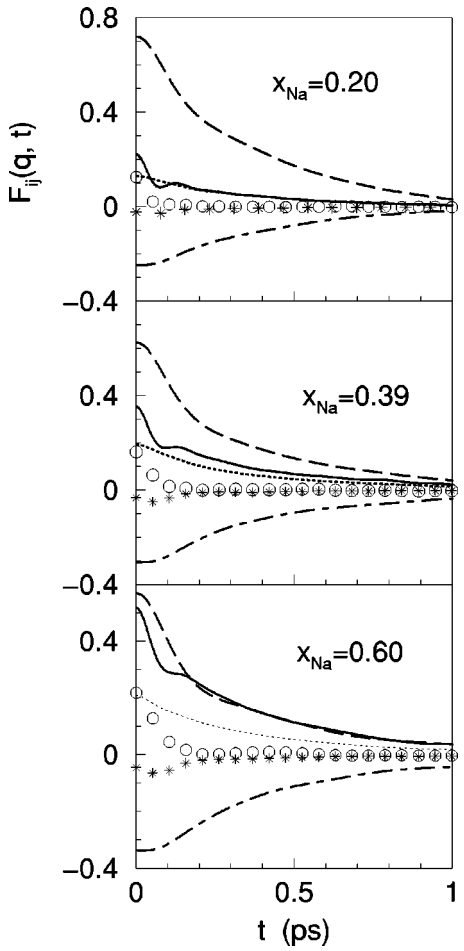

FIG. 5. Same as the previous figure, but for $q=1.50$ Å^{-1}.

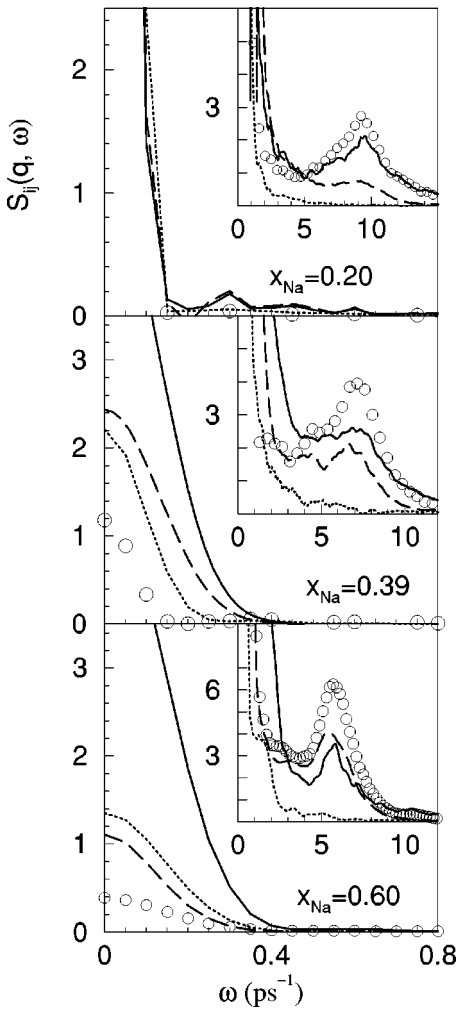

FIG. 6. Partial dynamic structure factors, $S_{ij}(q,\omega)$, at $q=0.23$ Å^{-1}, for the liquid Li-Na alloy at $T=590$ K and three concentrations. Full line—$S_{\mathrm{LiLi}}(q,\omega)$, dashed line—$S_{\mathrm{NaNa}}(q,\omega)$, circles—$S_{\mathrm{NN}}(q,\omega)$, and dotted line—$S_{\mathrm{CC}}(q,\omega)$. The insets show $10^3 S_{ij}(q,\omega)$.

$=4640\pm150$ m/s, respectively, which are close to the corresponding experimental values [58] of 2410 and 4450 m/s.

Whereas for the three concentrations $S_{\mathrm{LiLi}}(q,\omega)$ shows side peaks up to $q\approx1.30$ Å^{-1}, those of $S_{\mathrm{NN}}(q,\omega)$ and $S_{\mathrm{NaNa}}(q,\omega)$ depend on the concentration. The maximum q value for which peaks of $S_{\mathrm{NN}}(q,\omega)$ appear vary with concentration from $q\approx1.30$ Å^{-1} at $x_{\mathrm{Na}}=0.20$ to $q\approx0.85$ Å^{-1} at $x_{\mathrm{Na}}=0.60$, while in the case of $S_{\mathrm{NaNa}}(q,\omega)$ the maximum q for which peaks are present ranges from $q\approx0.40$ Å^{-1} at $x_{\mathrm{Na}}=0.20$ to $q\approx1.1$ Å^{-1} at $x_{\mathrm{Na}}=0.60$. From the positions of these side peaks, we have obtained dispersion curves, $\omega_{\mathrm{LiLi}}(q)$ and $\omega_{\mathrm{NaNa}}(q)$, which are shown in Fig. 8. Up to $q\approx0.25$ Å^{-1}, $\omega_{\mathrm{LiLi}}(q)$ and $\omega_{\mathrm{NaNa}}(q)$ show, for the three concentrations, the same linear behavior of hydrodynamic collective excitations propagating with the respective adiabatic velocities c_s. Above this q value, each dispersion curve splits into two branches indicating two modes, known as fast and slow sound modes, which signals the onset of a dynamic decoupling between the Li and Na particles. The fast mode, which involves the Li particles only, has a phase velocity, $c_{\mathrm{fast}}\approx3800\pm200$ m/s, which is roughly the same for the three concentrations. Furthermore, according to the predictions of the RET [12,13], the phase velocity associated with the fast mode should take a value very close to the adiabatic sound velocity of the corresponding light particle fluid, in this case a pure Li system obtained by substituting all the Na particles by Li particles. Consequently, we have performed OF-AIMD simulations for pure Li at 590 K and a total number density corresponding to the $Li_{0.61}Na_{0.39}$ alloy, and for which we obtained an adiabatic sound velocity of 3900 m/s, which is very close to the velocity of the fast mode. Denoting by q_h the upper limit of the hydrodynamic region, we stress that our results show that when q decreases towards q_h, the fast sound mode undergoes a continuous transition into the hydrodynamic sound mode and the process takes place at $0.2\leqslant q\leqslant0.4$ Å^{-1}. Furthermore, as discussed by Campa and Cohen, when the concentration of the light component is increased the fast mode will eventually disappear, being overcome by the extended sound mode. This can be observed in Fig. 8 where at $x_{\mathrm{Na}}=0.20$, the dispersion curve $\omega_{\mathrm{LiLi}}(q)$ is rather close to the extended hydrodynamic sound mode.

There has been some argument concerning the way in which the two kinetic modes behave when approaching q_h from above. Some theoretical and CMD results for He-Ar

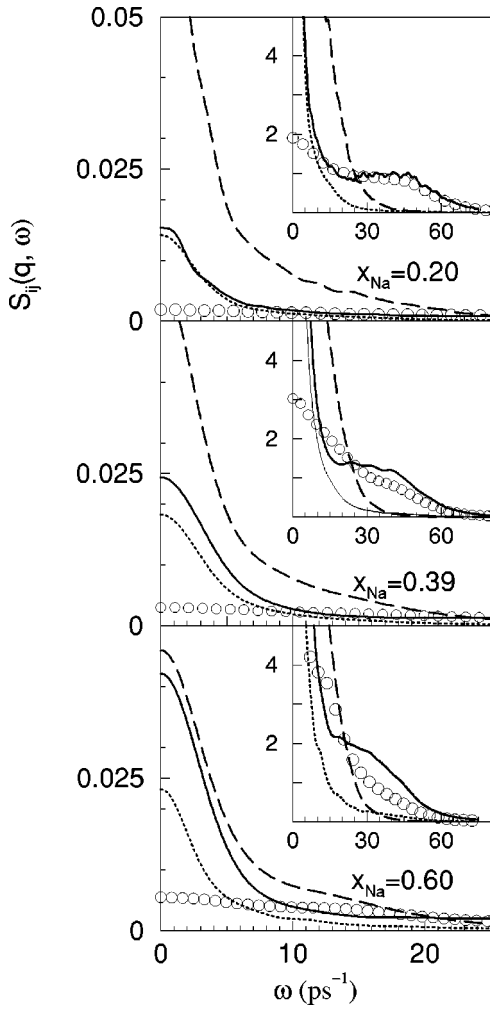

FIG. 7. Same as the previous figure, but for $q=1.50$ Å^{-1}.

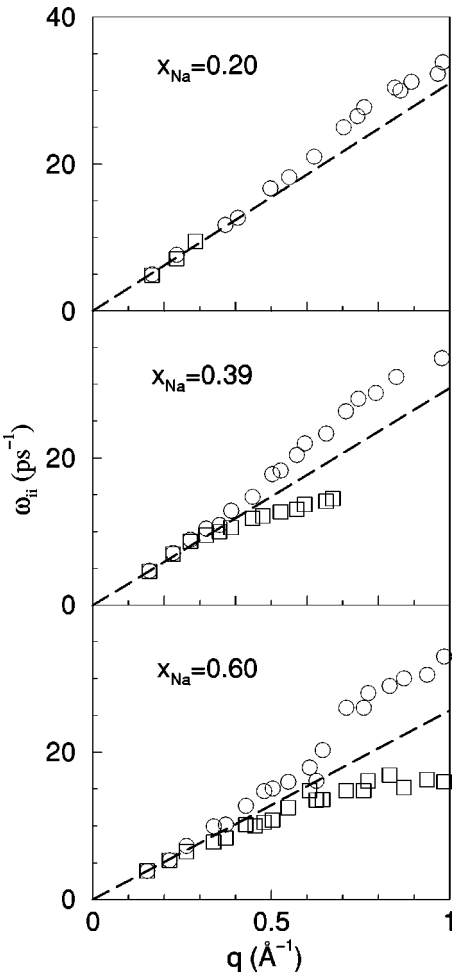

FIG. 8. OF-AIMD results for the dispersion curves of the collective modes in $S_{\mathrm{LiLi}}(q,\omega)$ and $S_{\mathrm{NaNa}}(q,\omega)$ (open circles and squares, respectively) for the liquid Li-Na alloy at $T=590$ K and three concentrations. The dashed line stands for the corresponding hydrodynamic adiabatic sound velocities.

and He-Ne mixtures have suggested that either the fast and slow sound merge into the hydrodynamic sound [15,21] or that the fast sound disappears at q_h, and the slow sound merges into the hydrodynamic one, with a predicted value [13,15,21] for $q_h \approx 0.07$ Å^{-1}. A similar value for q_h has recently been obtained for liquid Li_4Pb by both INS and by CMD calculations [16,24]. However, recent CMD calculations [18], following the INS measurements of Bafile *et al.* [57], for the dynamic structure of a $He_{0.77}Ne_{0.23}$ gas mixture at two densities, have shown a clear crossover from hydrodynamics to fast and slow modes at $0.2 \leqslant q \leqslant 0.5$ Å^{-1} and gave $q_h \approx 0.2$, which is substantially greater than previous estimates, and quantitatively agrees with the present results for the liquid Li-Na alloy.

Additional information on the longitudinal collective modes in liquids is provided by the longitudinal current correlation functions, $C^L_{ij}(q,\omega) \equiv \omega^2 S_{ij}(q,\omega)$. For example, although $S_{\mathrm{CC}}(q,\omega)$ shows neither side peaks nor shoulders at any q value because of the dominance of the diffusive contributions in the partial intermediate scattering functions, collective modes may be exposed in $C^L_{\mathrm{CC}}(q,\omega)$.

We have evaluated these functions, as given by Eq. (15), and they are shown in Figs. 9 and 10. For any q value, $C^L_{\mathrm{LiLi}}(q,\omega)$, $C^L_{\mathrm{NaNa}}(q,\omega)$, and $C^L_{\mathrm{NN}}(q,\omega)$ exhibit at least one peak, although when the hydrodynamic region is approached both $C^L_{\mathrm{LiLi}}(q,\omega)$ and $C^L_{\mathrm{NN}}(q,\omega)$ show two peaks for $x_{\mathrm{Na}}=0.39$ and 0.60, and a peak and a shoulder for $x_{\mathrm{Na}}=0.20$. At the smaller q values reached by the simulations, the peak in $C^L_{\mathrm{NaNa}}(q,\omega)$ as well as the low-frequency peaks of $C^L_{\mathrm{LiLi}}(q,\omega)$ and $C^L_{\mathrm{NN}}(q,\omega)$ are at the same positions as the Brillouin peaks in $S_{\mathrm{NaNa}}(q,\omega)$, $S_{\mathrm{LiLi}}(q,\omega)$, and $S_{\mathrm{NN}}(q,\omega)$, respectively. Moreover, at these low q values, the peaks in $C^L_{\mathrm{NaNa}}(q,\omega)$, $C^L_{\mathrm{LiNa}}(q,\omega)$ and the low-frequency peak of $C^L_{\mathrm{LiLi}}(q,\omega)$ appear at practically the same position (see Fig. 9), which is another indication of the hydrodynamic behavior of the Li and Na particles at these small q values. On the other hand, for $x_{\mathrm{Na}}=0.39$ and 0.60, the high-frequency peak of $C^L_{\mathrm{LiLi}}(q,\omega)$ occurs where $C^L_{\mathrm{LiNa}}(q,\omega)$ has a minimum, which suggests that the Li and Na particles oscillate out of phase in an opticlike mode.

The longitudinal dispersion relations, $\omega^L_{\mathrm{LiLi}}(q)$, $\omega^L_{\mathrm{NaNa}}(q)$, and $\omega^L_{\mathrm{NN}}(q)$, obtained from the positions of the peaks discussed above are shown in Fig. 11. Note that $\omega^L_{\mathrm{NaNa}}(q)$ takes

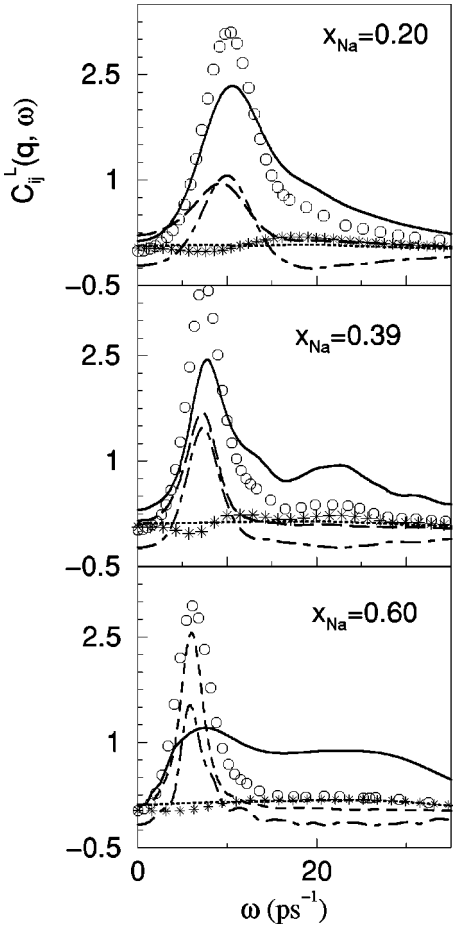

FIG. 9. Partial longitudinal current correlation functions, $C_{ij}^{L}(q,\omega)$, at $q=0.23$ Å^{-1}, for the liquid Li-Na alloy at $T=590$ K and three concentrations. Full line—$C_{\mathrm{LiLi}}^{L}(q,\omega)$, dashed line—$C_{\mathrm{NaNa}}^{L}(q,\omega)$, dot-dashed line—$C_{\mathrm{LiNa}}^{L}(q,\omega)$, open circles—$C_{\mathrm{NN}}^{L}(q,\omega)$, stars—$C_{\mathrm{NC}}^{L}(q,\omega)$, and dotted line—$C_{\mathrm{CC}}^{L}(q,\omega)$.

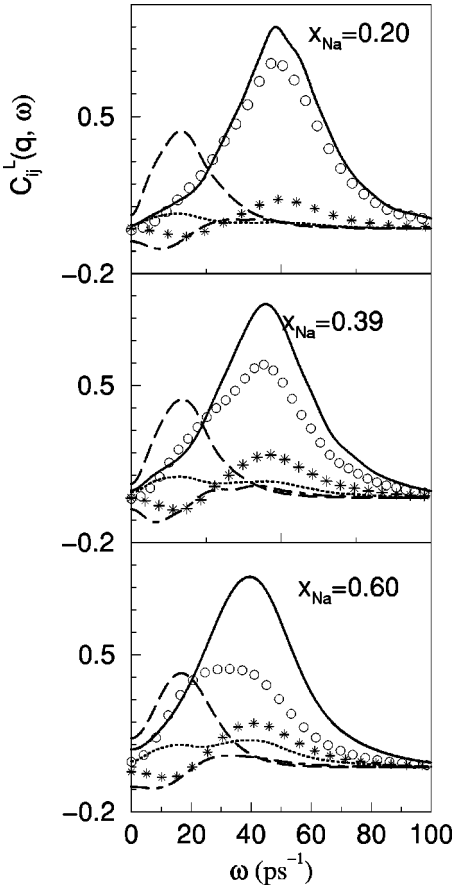

FIG. 10. Same as the previous figure, but for $q=1.50$ Å^{-1}.

smaller values than those of $\omega_{\mathrm{LiLi}}^{L}(q)$, because of the atomic mass difference. For all concentrations, $\omega_{\mathrm{NaNa}}^{L}(q)$ has one branch whereas $\omega_{\mathrm{LiLi}}^{L}(q)$ and $\omega_{\mathrm{NN}}^{L}(q)$ exhibit two for $x_{\mathrm{Na}}=0.39$ and 0.60, with the low-frequency branch, which has a limited extent, located at the low q's, close to the hydrodynamic region. This is because at these two concentrations (see Figs. 9 and 10), when q decreases, going towards the hydrodynamic regime, $C_{\mathrm{LiLi}}^{L}(q,\omega)$ and $C_{\mathrm{NN}}^{L}(q,\omega)$ develop two peaks, with the low-frequency peak being close to that of $C_{\mathrm{NaNa}}^{L}(q,\omega)$, and the high-frequency one taking values similar to those of the pure Li system. This suggests that in the binary alloy the heavy Na ions always keep their characteristic low frequencies whereas the light Li ions have a much higher frequency which is largely maintained when approaching the hydrodynamic regime, although as q decreases some Li ions adopt the low frequency of the heavy Na ions. Obviously, in the hydrodynamic ($q\rightarrow 0$) limit, all the particles oscillate with the same frequency and $C_{\mathrm{LiLi}}^{L}(q,\omega)$ and $C_{\mathrm{NN}}^{L}(q,\omega)$ only show the low-frequency peak; the high-frequency one will vanish.

As shown in Fig. 11, at low q values $\omega_{\mathrm{NaNa}}^{L}(q)$ has an initial linear increase up to a maximum followed by a minimum at $q\approx 2.0$ Å^{-1} which corresponds to the main peak position of $S_{\mathrm{NaNa}}(q)$. As x_{Na} increases, the main peak of $S_{\mathrm{NaNa}}(q)$ gets higher and narrower but at a fixed position; and therefore the first minimum of $\omega_{\mathrm{NaNa}}^{L}(q)$ becomes more marked. The high-frequency branch of $\omega_{\mathrm{LiLi}}^{L}(q)$ behaves similarly, with a maximum and minimum at ≈ 1.5 Å^{-1} and 2.3 Å^{-1}, respectively, which coincide with the first minimum and maximum of $S_{\mathrm{LiLi}}(q)$. Moreover as x_{Na} is increased the structure of $\omega_{\mathrm{LiLi}}^{L}(q)$ becomes less marked as happens with the maxima and minima in $S_{\mathrm{LiLi}}(q)$.

The $\omega_{\mathrm{NN}}^{L}(q)$ dispersion curve has two branches for $x_{\mathrm{Na}}=0.39$ and 0.60, although the high-frequency branch has a very limited extent close to the hydrodynamic region (see Fig. 11). At these low q values, the high-frequency branch is due to Li particles only, whereas the other comes from both Li and Na particles. For larger q, $C_{\mathrm{LiLi}}^{L}(q,\omega)$ becomes the main contributor to $C_{\mathrm{NN}}^{L}(q,\omega)$, and when Li is the majority component, $\omega_{\mathrm{LiLi}}^{L}(q)$ and $\omega_{\mathrm{NN}}^{L}(q)$ are rather close. In contrast, when Na is the majority component, $\omega_{\mathrm{NN}}^{L}(q)$ lies between $\omega_{\mathrm{NaNa}}^{L}(q)$ and $\omega_{\mathrm{LiLi}}^{L}(q)$.

$\omega_{\mathrm{CC}}^{L}(q)$ also has two branches because $C_{\mathrm{CC}}^{L}(q,\omega)$, which is smaller than the other partial currents especially at low q, shows either one or two peaks which may be connected with propagating concentration modes. The high-frequency branch of $\omega_{\mathrm{CC}}^{L}(q)$, which exists for all q values, closely follows the high-frequency branch of $\omega_{\mathrm{NN}}^{L}(q)$ and tends to a

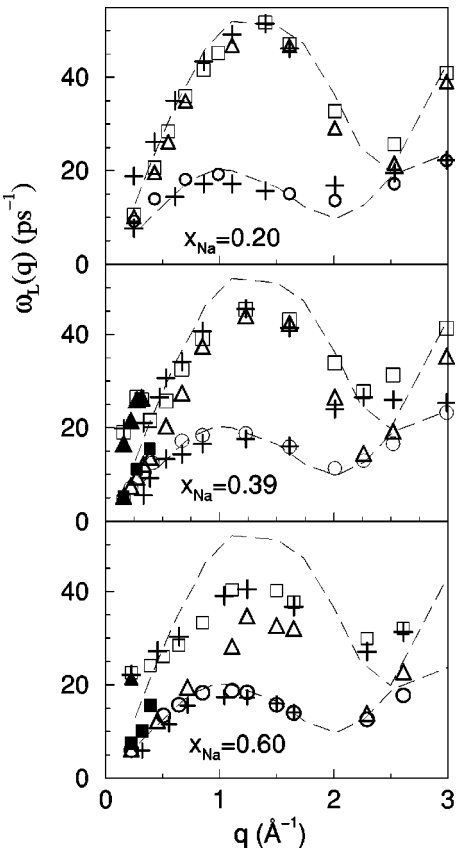

FIG. 11. Longitudinal dispersion relation of the partials, $\omega^L_{\mathrm{LiLi}}(q)$, (open and full squares), $\omega^L_{\mathrm{NaNa}}(q)$ (open circles), number-number, $\omega^L_{\mathrm{NN}}(q)$ (open and full triangles), and concentration-concentration, $\omega^L_{\mathrm{CC}}(q)$ (pluses) longitudinal modes for the Li-Na liquid alloy at $T=590$ K and three concentrations. The dashed lines show the longitudinal dispersion relations of pure Li and Na at $T=590$ K.

finite value when $q\to 0$, which is typical of kinetic modes. On the other hand, the low-frequency branch of $\omega^L_{\mathrm{CC}}(q)$ appears just outside the hydrodynamic regime and follows $\omega^L_{\mathrm{NaNa}}(q)$ closely.

Dispersion relations for pure Li and Na at $T=590$ K are also shown in Fig. 11. Notice that the dispersion relation for the majority component in the alloy is very close to that of the pure component; however, the dispersion relation of the minority component has less structure than that of the corresponding pure metal.

3. Total dynamic structure factor

The total dynamic structure factor $S_T(q,\omega)$ is directly related to the intensity obtained in either INS or IXS experiments. For the specific case of an INS experiment, the observed $S^n_T(q,\omega)$ is given by

$$\langle b^2\rangle S^n_T(q,\omega)=\sum_{i=1}^{2}(\langle b_i^2\rangle-\langle b_i\rangle^2)c_i S^s_i(q,\omega)+\sum_{i,j=1}^{2}(c_ic_j)^{1/2}\langle b_i\rangle\langle b_j\rangle S_{ij}(q,\omega), \quad (15)$$

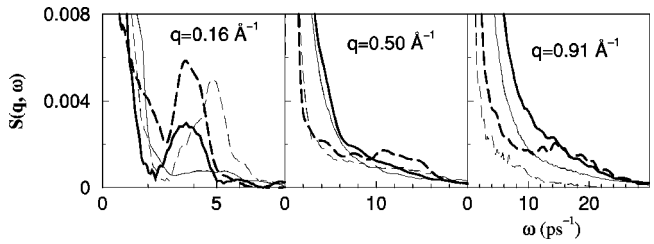

FIG. 12. Total dynamic structure factor for liquid Li-Na alloys. Full lines: neutron results. Dashed lines: x-rays results. Thick lines correspond to $x_{\mathrm{Na}}=0.60$ and thin lines to $x_{\mathrm{Na}}=0.20$.

where $S_{ij}(q,\omega)$ are AL partials, $S^s_i(q,\omega)$ are the self-dynamic partial structure factors, $\langle b_i\rangle$ is the coherent scattering length, $4\pi\langle b_i^2\rangle$ is the total scattering cross section, and $\langle b^2\rangle=\Sigma_{i=1}^2 c_i\langle b_i^2\rangle$ is the average cross section per atom. The first and second terms in Eq. (15) are the incoherent and coherent contributions, respectively. In the case of IXS experiments, the observed $S^X_T(q,\omega)$ is given by a similar expression but with no incoherent contribution and scattering lengths, b_i, replaced by the q-dependent atomic scattering factors, $f_i(q)$.

The total dynamic structure factor has been measured [29], using INS, for the zero alloy composition at $T=577$ and 725 K, leading to a monotonous decaying shape. Our simulations have confirmed this absence of side peaks which we have explained as due to the cancellation between the contributions from the LiNa partial structure factor and those from the LiLi and NaNa partials structure factors [20]. The simulation results for $S^n_T(q,\omega)$ are slightly larger than the experimental results. This behavior was noted earlier by Anento *et al.* [39] in their CMD simulations with NPA potentials, and explained in terms of the experimental uncertainties (limited ω range, inelasticity corrections) that led to a certain inconsistency between the experimental dynamic structure factor and the static counterpart. However, the IXS results for the zero alloy obtained from the simulations did show side peaks [20], mainly connected to those of the NaNa partial structure factor because of the larger magnitude of its prefactor.

Here we have extended these calculations to the other two concentrations $x_{\mathrm{Na}}=0.20,0.60$ and the results are shown in Fig. 12 for three q values. Two points are noteworthy: first, the neutron total dynamic structure factor does show side peaks in a limited q range, because the cancellation between the like and unlike partial structure factors is not complete (note the peak at $q=0.16$ Å^{-1} for both $x_{\mathrm{Na}}=0.20$ and 0.60, while there are no peaks at the larger wave vectors shown in the figure) and second, the x-ray total dynamic structure factor also displays side peaks in a similar or wider q range (note the peak at $q=0.16$ Å^{-1} for $x_{\mathrm{Na}}=0.20$ and the clear peaks at $q=0.16,0.50$, and 0.91 Å^{-1} for $x_{\mathrm{Na}}=0.60$), which depends on the concentration because of the previously discussed concentration dependence of the NaNa partial structure factor.

4. Transverse currents

The partial transverse current correlation functions, $C^T_{ij}(q,\omega)$, provide information about the existence of shear

modes in the system. There are few reports of studies of the transverse currents in liquids, and most of these have focused on one-component systems where $C^T(q,\omega)$ evolves [7] from a Gaussian, when $q\to\infty$, towards a Lorentzian curve when $q\to 0$. These extreme regimes preclude the propagation of transverse modes. However, at intermediate q values above some q_c, $C^T(q,\omega)$ exhibits a peak at nonzero frequency, which is associated with propagating shear waves.

The first CMD simulations of transverse current correlations in binary systems were performed on molten salts [59], and showed that $C^T_{\mathrm{NN}}(q,\omega)$ behaved similar to $C^T(q,\omega)$ in one-component liquids, with a peak at intermediate q values. Moreover, the charge-charge transverse current correlation functions showed a peak at both low and intermediate q's which was related to the existence of transverse optic modes whose frequencies take a finite value in the hydrodynamic $(q\to 0)$ limit. Later CMD studies of transverse modes in binary Lennard-Jones [14] systems have found opticlike modes associated with $C^T_{\mathrm{CC}}(q,\omega)$. Similar conclusions have also been reached by Anento and Padró [60] in their recent CMD studies of liquid Li-Mg, Li-Na, and Li-Pb alloys.

Results for $C^T_{ij}(q,\omega)$ are shown in Figs. 13 and 14. Neither $C^T_{\mathrm{NaNa}}(q,\omega)$ nor $C^T_{\mathrm{LiNa}}(q,\omega)$ have peaks at $q_{\min}$, although for larger q a peak appears in both partial currents and persists for a limited range of q values. Moreover, $C^T_{\mathrm{LiNa}}(q,\omega)$ falls quickly as q increases reflecting the rather weak coupling between the dynamics of the species. However, even at the corresponding $q_{\min}$, $C^T_{\mathrm{LiLi}}(q,\omega)$ at $x_{\mathrm{Na}}=0.60$ already exhibits a high-frequency peak which persists up to $q\approx 4$ Å^{-1}. Figures 13 and 14 also show $C^T_{\mathrm{NN}}(q,\omega)$ which for the three concentrations at their respective $q_{\min}$, decay monotonically, although a peak appears in a limited range at larger q.

The transverse dispersion relations, $\omega^T_{ij}(q)$, shown in Fig. 15, have been obtained from the peak positions of the corresponding $C^T_{ij}(q,\omega)$. For $q\geqslant 1$ Å^{-1}, $\omega^T_{\mathrm{LiLi}}(q)$ and $\omega^T_{\mathrm{NaNa}}(q)$, at the three concentrations, are roughly the same and the important changes appear at the low q region. However, whereas for all concentrations $\omega^T_{\mathrm{NaNa}}(q)$ goes to zero as $q\to 0$, when the lighter Li particles become the minority component $\omega^T_{\mathrm{LiLi}}(q)$ tends to a finite frequency as $q\to 0$.

The dispersion curve, $\omega^T_{\mathrm{NN}}(q)$, lies between $\omega^T_{\mathrm{LiLi}}(q)$ and $\omega^T_{\mathrm{NaNa}}(q)$ although closer to the majority component, and shows typical features of the one-component system, namely, it starts at a q_c ($q_c\approx 0.50$ Å^{-1} for $x_{\mathrm{Na}}=0.20$ and $q_c\approx 0.55$ Å^{-1} for $x_{\mathrm{Na}}=0.60$), exhibits a linear behavior for low q values and goes to zero as $q\to q_c$. The slope in the linear region assuming $\omega^T_{\mathrm{NN}}(q)\sim c_T(q-q_c)$ yields an estimate of the velocity of propagation of the shear modes in the alloy: $c_T\approx 3650$ m/s for $x_{\mathrm{Na}}=0.20$, $c_T\approx 1900$ m/s for $x_{\mathrm{Na}}=0.39$, and $c_T\approx 1600$ m/s for $x_{\mathrm{Na}}=0.60$. For the limiting cases of pure Li and Na at $T=590$ K, we have obtained $c_T\approx 3700$ m/s and $c_T\approx 1600$ m/s, respectively. For $x_{\mathrm{Na}}=0.20$ and 0.39, when the lighter Li particles are the majority, $\omega^T_{\mathrm{NN}}(q)$ is close in the linear region to both $\omega^T_{\mathrm{LiLi}}(q)$ and $\omega^T_{\mathrm{NaNa}}(q)$, implying that the propagation of shear modes involves both species. However, for $x_{\mathrm{Na}}=0.60$, $\omega^T_{\mathrm{LiLi}}(q)$ separates from the other two and is finite as $q\to 0$, which suggests that the shear modes will now propagate only through the heavier Na particles. This explains why c_T in the alloy is the same as that of pure Na.

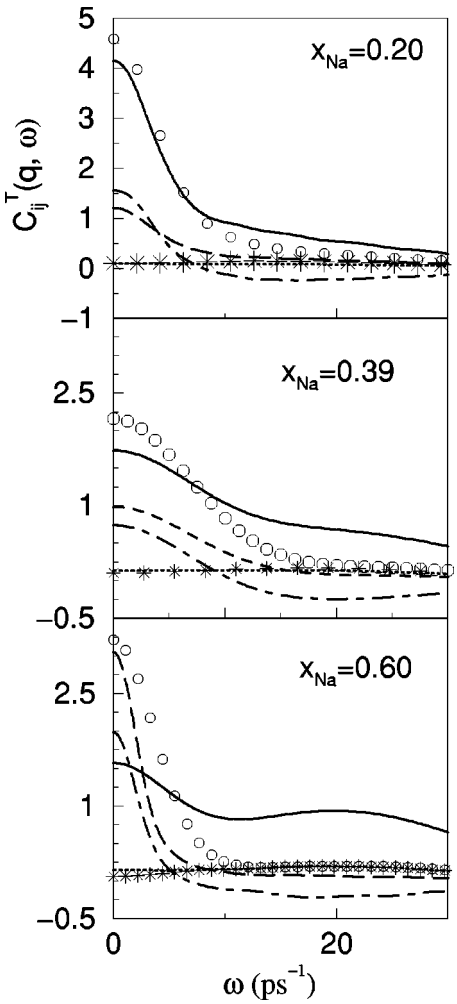

FIG. 13. Partial transverse current correlation functions, $C^T_{ij}(q,\omega)$, at $q=0.23$ Å^{-1}, for the liquid Li-Na alloy at $T=590$ K and three concentrations. Full line—$C^T_{\mathrm{LiLi}}(q,\omega)$, dashed line—$C^T_{\mathrm{NaNa}}(q,\omega)$, dot-dashed line—$C^T_{\mathrm{LiNa}}(q,\omega)$, open circles—$C^T_{\mathrm{NN}}(q,\omega)$, stars—$C^T_{\mathrm{NC}}(q,\omega)$, and dotted line—$C^T_{\mathrm{CC}}(q,\omega)$.

The small values taken by $C^T_{\mathrm{NC}}(q,\omega)$ suggest weak couplings between density and concentration modes. The small magnitude of $C^T_{\mathrm{CC}}(q,\omega)$, particularly at small q's, also signals a weak contribution to the collective transverse dynamics. However, for the three concentrations we observe clear peaks in $C^T_{\mathrm{CC}}(q,\omega)$ which already exist at $q_{\min}$, leading to an $\omega^T_{\mathrm{CC}}(q)$ branch which takes a finite value as $q\to 0$. The peaks in $C^T_{\mathrm{CC}}(q,\omega)$ are a result of a minimum in $C^T_{\mathrm{LiNa}}(q,\omega)$ which is related to out-of-phase motion of particles of different species. Similar behavior in molten salts has been associated with transverse optic modes of kinetic character [14,59]. Analogous results have been obtained by Bryk and Mryglod in their GCM study of the transverse dynamics in some liquid alloys [14], and also by Anento and Padró [60] in their CMD simulations of liquid Li-Mg, Li-Na, and Li_4Pb alloys. Our simulations also show another, low frequency,

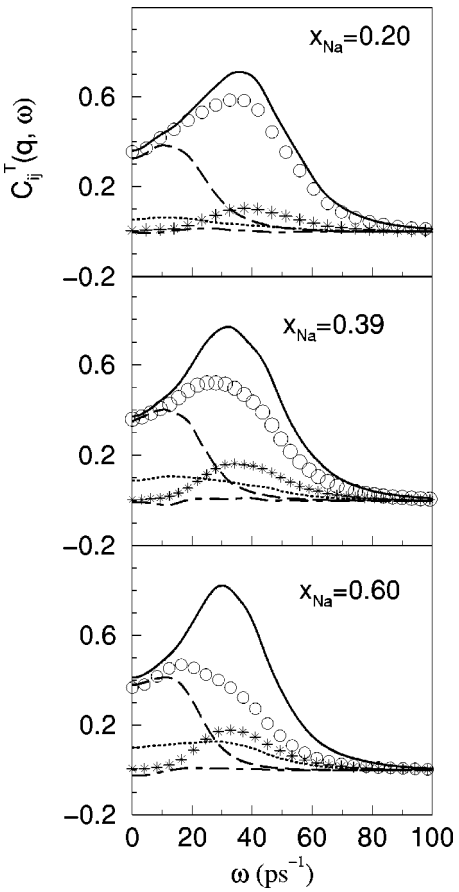

FIG. 14. Same as the previous figure, but for $q=1.50$ Å^{-1}.

$\omega^T_{CC}(q)$ branch starting well outside the linear region and associated with the shear modes, in accordance with the CMD results of Anento and Padró [60] for liquid $Li_{0.61}Na_{0.39}$. This suppression of the CC modes in the long-wavelength limit agrees with the predictions of the GCM model [14] for systems with a high mutual diffusion and a tendency towards homocoordination.

The alloy shear viscosity can be also derived from the previous results using the total transverse current correlation function $C^T_{tt}(q,t)=\langle j^T_t(q,t)j^{T*}_t(q,0)\rangle$, where $j^T_t(q,t)=x_1^{1/2}m_1j^T_1(q,t)+x_2^{1/2}m_2j^T_2(q,t)$ is the total transverse current and $j^T_i(q,t)$ are defined according to Eq. (13). In the hydrodynamic limit [7]

$$C^T_{tt}(q\to 0,t)=(\bar{m}/\beta)\exp\{-q^2\eta|t|/\bar{m}\rho\}, \qquad (16)$$

where $\bar{m}=x_1m_1+x_2m_2$ and η is the alloy shear viscosity. In its memory function representation

$$\tilde{C}^T_{tt}(q,z)=\frac{1}{\beta\bar{m}}\left[z+\frac{q^2}{\rho m}\tilde{\eta}(q,z)\right]^{-1}, \qquad (17)$$

where the tilde denotes the Laplace transform, a generalized alloy shear viscosity coefficient $\tilde{\eta}(q,z)$ is introduced. The area under the normalized $C^T_{tt}(q,t)$ gives $\beta\bar{m}\tilde{C}^T_{tt}(q,z=0)$, from which values for $\tilde{\eta}(q,z=0)$ are derived and, when extrapolated to $q=0$, give the alloy shear viscosity η. The

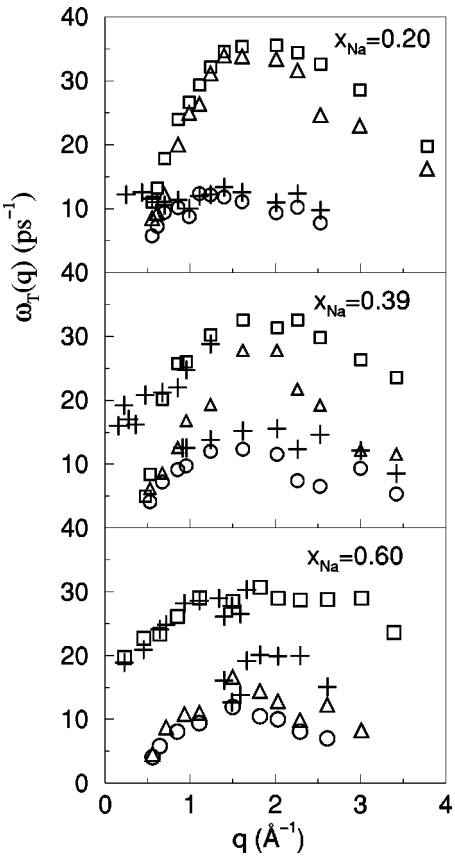

FIG. 15. Transverse dispersion relation of the partials, $\omega^T_{LiLi}(q)$ (open squares), $\omega^T_{NaNa}(q)$ (open circles), number-number, $\omega^T_{NN}(q)$ (open triangles), and concentration-concentration, $\omega^T_{CC}(q)$ (pluses) transverse modes for the Li-Na liquid alloy at $T=590$ K and three concentrations.

calculated values for η are shown in Table IV; those for pure Li and Na at $T=590$ K are in reasonable agreement with the experimental data [61] but no experimental data are yet available for the alloy.

For simple liquid alloys, η shows either a linear variation with concentration or a small negative deviation from linearity. In contrast, large positive deviations are exhibited by those alloys with heterocoordinating tendencies. For liquid alloys with homocoordinating tendencies, the available experimental data [47,62] show a mixed behavior with a negative departure from linearity predominating. Also, some

TABLE IV. Calculated values of the shear viscosity η (in GPa ps) for the Li-Na liquid alloy at $T=590$ K. The value in parenthesis corresponds to $T=725$ K.

x_{Na}	η	η_{expt}
0.0	4.0±0.3	4.3±0.2[a]
0.20	3.3±0.3	
0.39	3.1±0.3 (2.4±0.3)	
0.60	2.9±0.3	
1.0	3.2±0.3	3.3±0.2[a]

[a]Reference [61].

semiempirical models [53,62] give a connection between positive (negative) deviations from the linear law and a negative (positive) enthalpy of mixing in the alloy. Although no experimental data are available for the enthalpy of mixing, several theoretical calculations [31–33] have predicted positive values which, combined with the previous semiempirical models, would suggest a negative deviation of the alloy shear viscosity from a linear law. This is the trend in the results of the simulation shown in Table IV, in qualitative agreement with expectations for a homocoordinating tendency in the alloy.

IV. CONCLUSIONS

We have calculated several static and dynamic properties of the liquid $Li_{1-x}Na_x$ alloy at three concentrations. The simulations have been performed using the orbital-free *ab initio* molecular dynamics method combined with local pseudopotentials derived within the same framework. The method approximates the electron kinetic energy and in such is inferior to the full Kohn-Sham *ab initio* approach. However, it is very much faster allowing simulation of much larger systems for longer times. Several time correlation functions have been calculated and a comprehensive study of the dynamical properties of the binary alloy has been achieved. Similar molecular dynamics studies have been reported using interatomic pair potentials but these do not take into account effects of fluctuations in the electron density. The present approach takes account of these effects which will be considerable in the alloy we have studied because although Li and Na have the same valence they have very different sizes.

The results for static structural properties are in good agreement with the available experimental data, accounting satisfactorily for the homocoordinating tendencies in the alloy. The present calculations correctly give a high $S(q\rightarrow 0)$ as well as the splitting of the main peak appearing at $x_{\mathrm{Na}}=0.39$.

In studying the dynamical properties we have analyzed several time correlation functions, although comparison with experiment could only be made at the level of some transport coefficients. The calculated values for self-diffusion coefficients are in very good agreement with the available experimental data. The calculated partial dynamic structure factors, $S_{\mathrm{LiLi}}(q,\omega)$ and $S_{\mathrm{NaNa}}(q,\omega)$, show clear side peaks which extend far beyond the hydrodynamic regime and represent two nonhydrodynamic modes: the fast and slow sound modes, respectively. Although this phenomenon was predicted by the RET applied to a binary mixture of hard spheres [12], it was concluded that a mass ratio larger than 10 would be required for appearance of the nonhydrodynamic modes. The present calculations show that those modes may appear in systems with a smaller mass ratio, ≈ 3. Furthermore, we find that as the wave vector q approaches the hydrodynamic region, the fast sound mode smoothly merges into the hydrodynamic sound mode at around $0.2 \leqslant q \leqslant 0.4$ Å^{-1}.

The calculated longitudinal dispersion relation shows the existence of kinetic concentration modes. In addition, the calculated adiabatic sound velocity is in very good agreement with experiment for the limiting case of the pure components. Also noteworthy is the appearance of two branches in the transverse dispersion relation for $\omega^{T}_{\mathrm{CC}}(q)$, with the high-frequency branch representing overdamped kinetic modes. The low-frequency $\omega^{T}_{\mathrm{CC}}(q)$ branch appears just outside the linear region and does not exist for low q values. This behavior is consistent with the predictions of the GCM model.

The total neutron dynamic structure factor for the zero alloy is in qualitative agreement with the measured one [29], but the possibility that the experimental data are somewhat low, is suggested. Moreover, we predict that measurements at other concentrations would reveal visible side peaks at small wave vectors. The total x-ray dynamic structure factor, on the other hand, shows clear side peaks for a similar or wider wave vector range following the behavior of the NaNa partial structure factor, and an IXS experiment should show the slow sound mode related to this peak.

The shear viscosity of the alloy has been estimated using its connection to the hydrodynamic limit of the total transverse current correlation function. The results are plausible in view of the homocoordinating tendencies of this alloy and the positive enthalpy of mixing obtained by several models.

The main approximations in the present orbital-free *ab initio* molecular dynamics method are in the electron kinetic energy functional and the local pseudopotentials describing the electron-ion interactions. Further improvements in this method will come from the development of more accurate kinetic energy functionals and accurately transferable local pseudopotentials.

ACKNOWLEDGMENTS

Work was supported by the Junta de Castilla y León (Project No. VA073/02) and the DGES (Grant No. MAT2002-04393-C0201). D.J.G. gratefully acknowledges the financial support of both the Ministerio de Educacion, Cultura y Deportes of Spain and the Physics Department at Queen's University. M.J.S. acknowledges the support of the NSERC of Canada.

[1] P. Hohenberg and W. Kohn, Phys. Rev. **136**, B864 (1964).
[2] W. Kohn and L.J. Sham, Phys. Rev. **140**, A1133 (1965).
[3] F. Shimojo, Y. Zempo, K. Hoshino, and M. Watabe, J. Non-Cryst. Solids **205-207**, 983 (1996); B.J. Costa Cabral and J.L. Martins, Phys. Rev. B **51**, 872 (1995).
[4] G. Kresse, J. Non-Cryst. Solids **205-207**, 833 (1996); G. Kresse and J. Hafner, Phys. Rev. B **55**, 7539 (1997).
[5] Y. Senda, F. Shimojo, and K. Hoshino, J. Phys. Soc. Jpn. **67**, 2753 (1998).
[6] B.J. Costa Cabral and J.L. Martins, J. Chem. Phys. **111**, 5067 (1999).
[7] U. Balucani and M. Zoppi, *Dynamics of the Liquid State* (Clarendon, Oxford, 1994); J.P. Hansen and I.R. McDonald, *Theory of Simple Liquids* (Academic, London, 1986); J.P. Boon and S.

Yip, *Molecular Hydrodynamics* (McGraw-Hill, New York, 1980).
[8] L. Sjögren and A. Sjölander, J. Phys. C **12**, 4369 (1979); L. Sjögren, *ibid.* **13**, 705 (1980); Phys. Rev. A **22**, 2866 (1980); **22**, 2883 (1980).
[9] J. Casas, D.J. González, L.E. González, M.M.G. Alemany, and L.J. Gallego, Phys. Rev. B **62**, 12 095 (2000).
[10] G. Jacucci and I.R. McDonald, J. Phys. F: Met. Phys. **10**, L15 (1980).
[11] G. Jacucci, M. Ronchetti, and W. Schirmacher, J. Phys. (Paris) **46**(C-8), 385 (1985).
[12] A. Campa and E.G.D. Cohen, Phys. Rev. A **41**, 5451 (1990).
[13] P. Westerhuijs, W. Montfrooij, L.A. de Graaf, and I.M. de Schepper, Phys. Rev. A **45**, 3749 (1992).
[14] T. Bryk, I. Mryglod, and G. Kahl, Phys. Rev. E **56**, 2903 (1997); T. Bryk and I. Mryglod, Phys. Lett. A **261**, 349 (1999); J. Phys.: Condens. Matter **12**, 6063 (2000).
[15] E. Enciso, N.G. Almarza, P. Dominguez, M.A. González, and F.J. Bermejo, Phys. Rev. Lett. **74**, 4233 (1995).
[16] R. Fernández-Perea, M. Alvarez, F.J. Bermejo, P. Verkerk, B. Roessli, and E. Enciso, Phys. Rev. E **58**, 4568 (1998).
[17] N. Anento and J.A. Padro, Phys. Rev. B **62**, 11 428 (2000).
[18] M. Sampoli, U. Bafile, E. Guarini, and F. Barocchi, Phys. Rev. Lett. **88**, 085502 (2002).
[19] L.E. González, D.J. González, and J.M. López, J. Phys.: Condens. Matter **13**, 7801 (2001); J. Blanco, D.J. González, L.E. González, J.M. López, and M.J. Stott, Phys. Rev. E **67**, 041204 (2003).
[20] D.J. González, L.E. González, J.M. López, and M.J. Stott, Europhys. Lett. **62**, 42 (2003).
[21] R.M. Crevecoeur, H.E. Smorenburg, and I.M. de Schepper, J. Low Temp. Phys. **105**, 149 (1996).
[22] W. Montfrooij, P. Westerhuijs, V.O. de Haan, and I.M. de Schepper, Phys. Rev. Lett. **63**, 544 (1989).
[23] P.H.K. de Jong, P. Verkerk, C.F. de Vroege, L.A. de Graaf, W.S. Howells, and S.M. Bennington, J. Phys.: Condens. Matter **6**, L681 (1994).
[24] M. Alvarez, F.J. Bermejo, P. Verkerk, and B. Roessli, Phys. Rev. Lett. **80**, 2141 (1998).
[25] F.A. Kanda, R.C. Faxon, and D.V. Keller, Phys. Chem. Liq. **1**, 61 (1968).
[26] H.K. Schurmann and R.D. Parks, Phys. Rev. Lett. **27**, 1790 (1971).
[27] P.D. Feitsma, J.J. Hallers, F.V.D. Werff, and W. van der Lugt, Physica B **79**, 35 (1975).
[28] H. Ruppersberg and W. Knoll, Z. Naturforsch. A **32**, 1374 (1977).
[29] P.R. Gartrell-Mills, R.L. McGreevy, and W. van der Lugt, Physica B **154**, 1 (1988).
[30] V.K. Ratti and A.B. Bhatia, Nuovo Cimento Soc. Ital. Fis., B **43B**, 1 (1978).
[31] K. Hoshino and W.H. Young, J. Phys. F: Met. Phys. **16**, 1671 (1986); D.J. González and M. Silbert, *ibid.* **18**, 2353 (1988); J. Hafner and W. Jank, *ibid.* **18**, 333 (1988).
[32] D. Stroud, Phys. Rev. B **9**, 396 (1974); N.W. Ashcroft and D. Stroud, Solid State Phys. **33**, 1 (1978).
[33] J. Hafner and F. Sommer, CALPHAD: Comput. Coupling Phase Diagrams Thermochem. **1**, 325 (1977).
[34] K. Hoshino, M. Silbert, A. Stafford, and W.H. Young, J. Phys. F: Met. Phys. **17**, L49 (1987).
[35] K. Hoshino and J.J. van Wering, J. Phys. F: Met. Phys. **18**, L23 (1988).
[36] M. Canales, D.J. González, L.E. González, and J.A. Padró, Phys. Rev. E **58**, 4747 (1998).
[37] H. Mori, K. Hoshino, and M. Watabe, J. Phys. Soc. Jpn. **61**, 1218 (1992).
[38] D.J. González, L.E. González, M. Silbert, and J.A. Alonso, J. Phys.: Condens. Matter **5**, 4283 (1993).
[39] N. Anento, J. Casas, M. Canales, D.J. González, L.E. González, and J.A. Padró, J. Non-Cryst. Solids **250-252**, 348 (1999).
[40] F. Perrot, J. Phys.: Condens. Matter **6**, 431 (1994); E. Smargiassi and P.A. Madden, Phys. Rev. B **49**, 5220 (1994); M. Foley and P.A. Madden, *ibid.* **53**, 10 589 (1996).
[41] P. García-González, J.E. Alvarellos, and E. Chacón, Phys. Rev. A **54**, 1897 (1996); Phys. Rev. B **53**, 9509 (1996); **57**, 4857 (1998).
[42] J. Jost, D. Heydt, J. Spehr, and H. Ruppersberg, J. Phys.: Condens. Matter **6**, 321 (1994).
[43] D.J. González, L.E. González, J.M. López, and M.J. Stott, Phys. Rev. B **65**, 184201 (2002).
[44] L.E. González, A. Meyer, M.P. Iñiguez, D.J. González, and M. Silbert, Phys. Rev. E **47**, 4120 (1993).
[45] B.E. Warren, *X-Ray Diffraction* (Addison-Wesley, Reading, MA, 1969).
[46] J.M. Cowley, Phys. Rev. **77**, 667 (1950).
[47] R.N. Singh and F. Sommer, Rep. Prog. Phys. **60**, 57 (1997).
[48] R.L. McGreevy, A. Baranyai, and I. Ruff, Phys. Chem. Liq. **16**, 47 (1986).
[49] A.B. Bhatia and D.E. Thornton, Phys. Rev. B **2**, 3004 (1970).
[50] J. Trullás and J.A. Padró, J. Chem. Phys. **99**, 3983 (1993); Phys. Rev. E **50**, 1162 (1994).
[51] T. Kato, J. Phys. Chem. **89**, 5750 (1985).
[52] A. Feinauer and G. Majer, Phys. Rev. B **64**, 134302 (2001).
[53] M. Gerl and A. Bruson, in *Handbook of Thermodynamic and Transport Properties of Alkali Metals*, edited by R.W. Oshe (Blackwell, Oxford, 1985), p. 843.
[54] P.H.K. de Jong, Ph.D. thesis, Technische Universiteit Delft, 1993; A. Feinauer, G. Majer, and A. Seeger, J. Phys.: Condens. Matter **6**, L355 (1994).
[55] L.S. Darken and R.W. Gurry, *Physical Chemistry of Metals* (McGraw-Hill, New York, 1953).
[56] N.H. March and M.P. Tosi, *Atomic Dynamics in Liquid* (Dover, New York, 1991).
[57] U. Bafile, P. Verkerk, E. Guarini, and F. Barocchi, Phys. Rev. Lett. **86**, 1019 (2001).
[58] R.T. Beyer, in *Handbook of Thermodynamic and Transport Properties of Alkali Metals*, edited by R.W. Ohse (Blackwell, Oxford, 1985), p. 525.
[59] E.M. Adams, I.R. McDonald, and K. Singer, Proc. R. Soc. London, Ser. A **357**, 37 (1977).
[60] N. Anento and J.A. Padró, Mol. Mater. **99**, 275 (2001).
[61] E.E. Shpil'rain, K.A. Yakimovich, V.A. Fomin, S.N. Skovorodjko, and A.G. Mozgovoi, in *Handbook of Thermodynamic and Transport Properties of Alkali Metals*, edited by R.W. Ohse (Blackwell, Oxford, 1985), p. 753.
[62] M. Shimoji and I. Itami, *Atomic Transport in Liquid Metals* (Trans. Tech., Aedermannsdorf, 1986).